

Formation of η -mesic nuclei by the (π, N) reaction and properties of $N^*(1535)$ in mediumHideko Nagahiro,^{1,*} Daisuke Jido,² and Satoru Hirenzaki³¹Research Center for Nuclear Physics (RCNP), Osaka University, Ibaraki, Osaka, 567-0047, Japan²Yukawa Institute for Theoretical Physics, Kyoto University, Kyoto 606-8502, Japan³Department of Physics, Nara Women's University, Nara, 630-8506, Japan

(Received 30 November 2008; published 19 August 2009; publisher error corrected 3 September 2009)

We calculate formation spectra of the η -nucleus systems in the (π, N) reactions with nuclear targets, which can be performed at existing and/or forthcoming facilities, including the Japan Proton Accelerator Research Complex, to investigate the η -nucleus interaction. Based on the $N^*(1535)$ dominance in the ηN system, the η -mesic nuclei are suitable systems for the study of in-medium properties of the $N^*(1535)$ baryon resonance, such as reduction of the mass difference of N and N^* in the nuclear medium, which affects the level structure of the η and N^* -hole modes. We find that clear information on the in-medium N^* - and η -nucleus interactions can be obtained through the formation spectra of the η -mesic nuclei. We also discuss the experimental feasibilities by showing several spectra of the (π, N) reactions calculated with possible experimental settings. Coincident measurements of the $N\pi$ pairs from the N^* decays in nuclei help us to reduce backgrounds.

DOI: [10.1103/PhysRevC.80.025205](https://doi.org/10.1103/PhysRevC.80.025205)

PACS number(s): 21.85.+d, 21.65.Jk, 12.39.Fe, 14.20.Gk

I. INTRODUCTION

The study of meson-nucleus bound systems is one of the important subjects in nuclear physics. The detailed investigations of the structure of the bound states provide us quantitative information on the hadron-nucleus interactions. So far, the structure of atomic states of pion, kaon, Σ^- , and \bar{p} have been successfully observed and investigated comprehensively both in theoretical and experimental points of view [1]. One of the remarkable developments in experimental aspects is the establishment of the $(d, ^3\text{He})$ spectroscopy for the formation of deeply bound pionic atoms with recoil-free kinematics [2–5]. It opens new possibilities of the formation of other hadron-nucleus bound systems [6–10].

Bound states of the η meson in nuclei were predicted first by Haider and Liu [11]. After that, many works were devoted to studies of the structure of the bound states, the formation reactions of the η -mesic nuclei, and in-medium properties of the η meson [6,7,9,10,12–21]. Especially, the η meson in the nuclear medium has been recently investigated in the aspect of chiral symmetry [6,7,9,10,15–18,20]. The η -nucleus system is purely governed by strong interaction in contrast to the atomic states of mesons with negative charge. Thus, the η mesons in the bound states are largely overlapped with nuclei. In such compact systems, large medium effects on the mesons inside nuclei are expected, and, at the same time, wide natural widths of the bound states due to absorption of the mesons into the nucleus are inevitable, as seen in deeply bound kaonic nuclei [22].

The first experimental search of the η bound states in nuclei [23] was performed in the (π^+, p) reaction with several nuclear targets in finite momentum transfer to aim to observe narrow states as predicted in Ref. [11], and the result turned out to be

negative. Some hints of the η bound states were also observed as enhancement at the subthreshold of the η -meson production in $d(p, ^3\text{He})\eta$ [24] and $^{18}\text{O}(\pi^+, \pi^-)^{18}\text{Ne}$ [25] reactions. Observation of an η -meson bound state in ^3He was reported in photoproduction reactions [26], though interpretation of these observations are still controversial [27]. It was suggested in Ref. [28] that the coincident observation of the $N\pi$ pair from $N^*(1535)$ helps to identify the formation of η -meson bound states. Very recently, Ref. [29] has reported a hint of an η -nuclear bound state observed in the $^{27}\text{Al}(p, ^3\text{He})$ reaction with the coincident detection of $\pi^- p$. Other experiments have been also proposed [30–32].

The study of the hadron properties in the nuclear medium is largely related to the fate of chiral symmetry in finite density. It is expected that partial restoration of chiral symmetry in the nuclear medium takes place as reduction of the quark condensates [33,34] and provides an effective change of the hadron properties. For the context of the study of the η meson in the nuclear medium, the $N^*(1535)$ resonance, which can be a candidate of the chiral partner of the nucleon becoming degenerate in the chiral restoration limit [35–37], plays an important role in the η -mesic nuclei due to the strong coupling of the η -nucleon system to the $N^*(1535)$ resonance. In our previous works [9,10,18], it was found that the η optical potential in nuclei is strongly sensitive to the in-medium mass gap of N and $N^*(1535)$ and that, as a consequence, the formation spectra of the η -mesic nuclei is also sensitive to the in-medium properties of $N^*(1535)$.

The sensitivity of the η -nucleus optical potential to the N - N^* mass gap stems from possible level crossing between N^* -hole and η modes in the nuclear medium as suggested in Ref. [20]. The level difference between the N^* -hole and η modes without medium effects is only 50 MeV, which is 10% of the N - N^* mass gap and small enough in energy scale of hadronic interactions. We found that the level crossing caused by the reduction of the mass gap provides deep η bound states and significant enhancement of the formation spectra of the η -mesic nuclei in the quasifree η production energies. This

*Present address: Department of Physics, Nara Women's University, Nara 630-8506, Japan.

will be a clue to deduce the in-medium N^* properties in the η -mesic nuclei.

As for the study of the in-medium properties of the N^* resonance, there have been some theoretical and experimental studies of η production off nuclei such as (γ, η) reactions [38–44]. One of the theoretical works reported that the η photoproduction experiments are explained with small medium effects on $N(1535)$ [42]. The η photoproduction experiments have suggested that the η production scales as $A^{2/3}$ [38,45], where A is the nuclear mass number. This implies strong final-state interactions of the η meson in nuclei and/or the η meson production only at the nuclear surface.

The η production processes have different kinematics from the nucleon kick-out reactions for the formation of the η -nucleus bound systems, in which the η mesons can be produced at subthreshold energies. Thus, the formation of the η -mesic nuclei, which we discuss in this article, gives complementary information on the η -binding energy region, which is not accessible by the η -production reaction off the nuclei. In addition, the missing mass spectra of the (π, N) reactions can probe the absorption processes of the η meson into the nuclei. This is also one of the different points from the η productions.

In this article, we revisit the (π, N) reactions with the recoil-free kinematics for the formation of the η -mesic nuclei to get clearer information on the level structure of the η and N^* -hole modes and in-medium properties of $N^*(1535)$ in the viewpoint of the chiral symmetry for baryons. We will find that the appropriate kinetic energy of the injecting pion in this reaction can be attained by the Japan Proton Accelerator Research Complex (J-PARC) facility. We will also compare our calculation with the old experiment of the (π^+, p) reaction with finite momentum transfer [23], in which the peak structures predicted in Ref. [11] were not found. In this article, we discuss more appropriate experimental conditions than the old experiment. We also propose the coincident observation to reduce the large background shown in Ref. [23].

This article is organized as follows. In Sec. II, we discuss the properties of the η spectral functions in nuclear matter. In Sec. III, we introduce the η -nucleus optical potentials with a finite size nucleus and discuss their features. The formation spectra of the η -mesic nuclei will be shown in Sec. IV, and the physical meaning of the formation spectra will be discussed. In Sec. V we will discuss the experimental feasibilities, and finally, we will devote Sec. VI to summary of this article.

II. LEVEL CROSSING OF THE η -MESON AND N^* -HOLE MODES

In this section, we briefly review the interesting feature of the η meson in the nuclear medium [20]. The in-medium η propagator is given by

$$D_\eta(\omega, k; \rho)^{-1} = \omega^2 - k^2 - m_\eta^2 - \Pi_\eta(\omega, k; \rho), \quad (1)$$

where ω and k denote the energy and momentum of the η meson, m_η is its mass, and Π_η denotes the η self-energy in the nuclear medium. Thanks to the strong coupling of the ηN system to the $N^*(1535)$ resonance, we can evaluate the η self-

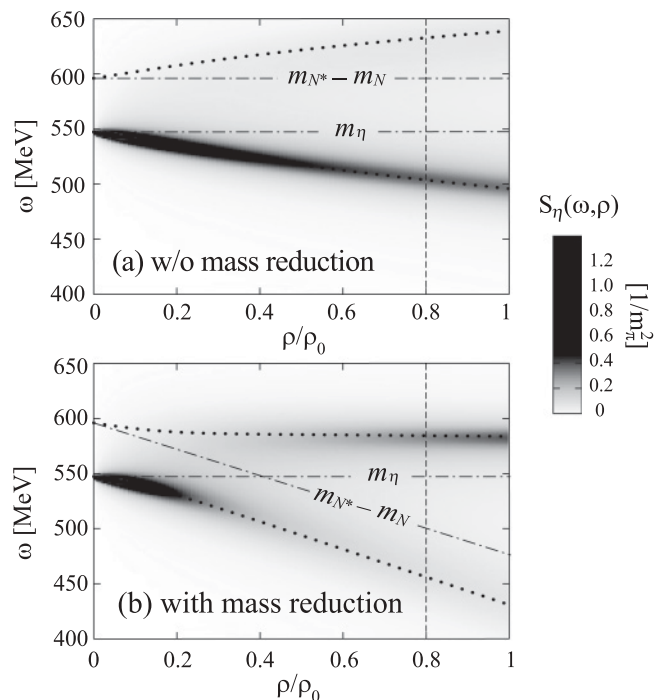


FIG. 1. Contour maps of the η meson spectral density in nuclear matter in Eq. (3) as functions of the baryon density and the η energy, assuming (a) the N and N^* masses not to change in medium and (b) 20% mass gap reduction of N and N^* at normal nuclear density ρ_0 . In this figure, the N^* width in medium is fixed to be constant $\Gamma_{N^*} = 75$ MeV for simplicity. The dotted lines indicate the real parts of the solutions of $D_\eta(\omega, k = 0; \rho)^{-1} = 0$ in Eq. (1).

energy by using the N^* dominance hypothesis. Considering the lowest N^* -nucleon-hole excitation, we obtain the η self-energy in small η momentum [9,20] as

$$\Pi_\eta(\omega, k; \rho) = \frac{g_\eta^2 \rho}{\omega + m_N^*(\rho) - m_{N^*}^*(\rho) + i\Gamma_{N^*}(\omega, \rho)/2} + (\text{crossed term}). \quad (2)$$

Here, g_η is the coupling constant of the s -wave ηNN^* vertex and can be determined as $g_\eta \simeq 2.0$ to reproduce the in-vacuum partial width $\Gamma_{N^* \rightarrow \eta N} \simeq 75$ MeV [46] at tree level. $m_N^*(\rho)$ and $m_{N^*}^*(\rho)$ are effective masses (free mass plus medium self-energy) of N and N^* in the nuclear medium with density ρ , respectively.

The η propagator (1) with the self-energy (2) has two poles with a positive real part in the complex energy plane in each density. These poles represent the η meson and N^* -hole modes in the nuclear medium [15,16,20]. Corresponding to these poles, the η spectral density S_η given by

$$S_\eta(\omega, \rho) = -\frac{1}{\pi} \text{Im}[D_\eta(\omega, k = 0; \rho)] \quad (3)$$

has two peaks in a function of real energy at a certain density.

We show the contour maps of the η spectral density as functions of baryon density and η energy in Fig. 1, where the real parts of the pole positions are indicated by the dotted lines. Figure 1(a) shows the strength of two branches in the case that the effective masses of N and N^* do not change in

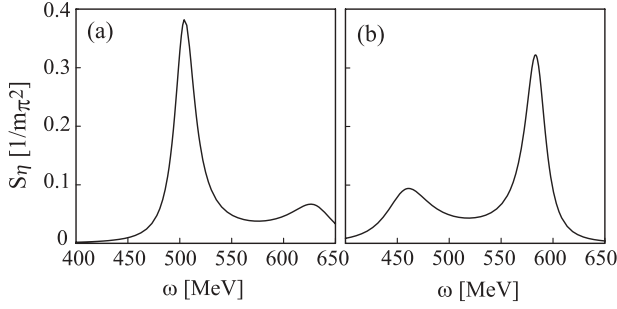


FIG. 2. Spectral functions of the η meson in nuclear matter as functions of the η energy at $\rho/\rho_0 = 0.8$ (indicated by the vertical dashed lines in Fig. 1) (a) without mass shift and (b) with 20% mass gap reduction of N^* and N at normal nuclear density.

medium. In this case, the two branches slightly come away from each other for higher ρ as a result of level repulsion, and the strength of the lower mode is always larger than the upper mode as also shown explicitly in Fig. 2(a). The similar behavior of the η spectral function based on the chiral unitary approach were also reported in Refs. [15,16], where the reduction of the mass gap between N and N^* is very small. In contrast, in the case that the mass gap becomes smaller in the nuclear medium, the behavior of the η spectral density significantly changes. Suppose that the mass gap of N and N^* linearly decreases by 20% at ρ_0 , the level crossing between the two branches takes place around $\rho \sim 0.4\rho_0$ as shown in Fig. 1(b). As a consequence, the strength of the upper mode becomes stronger due to the level mixing, and the lower mode shifts downward considerably as the density increases.

A possible source of the mass gap reduction is the partial restoration of chiral symmetry in the nuclear medium. If $N^*(1535)$ is a chiral partner of nucleon, the N and N^* mass difference should decrease as chiral symmetry is being restored. In this article, we use the following parametrization of the mass gap reduction based on the chiral doublet model [36,37]:

$$m_{N^*}^*(\rho) - m_N^*(\rho) = \left(1 - C \frac{\rho}{\rho_0}\right) (m_{N^*} - m_N), \quad (4)$$

where m_N and m_{N^*} are the N and N^* masses in free space, respectively. Here the parameter C represents the strength of the chiral restoration at the normal nucleon saturation density ρ_0 , and its empirical value lies from 0.1 to 0.3 [47]. Figures 1(b) and 2(b) correspond to the case with $C = 0.2$ ¹ in the chiral doublet model. These characteristic phenomena caused by the level crossing can be a signal of the reduction of the N and N^* mass gap, which supports the partial restoration of the chiral symmetry in the nuclear medium. In next section, we introduce the η -nucleus optical potentials for the study in finite size systems.

It is interesting that the upper level stays at very similar energy with the N^* -hole mode in low densities and has more strength than the lower level, as seen in Fig. 2(b).

¹ $C = 0.2$ is consistent with the calculation of the chiral condensate done in Ref. [48].

This mode could be seen in the η photoproduction in which the spectrum shapes are very similar with that observed in the deuteron target. Thus, the strong attraction for the N^* in the nuclear medium does not contradict the η photoproduction experiments yet. For further investigation, one needs to calculate the η photoproduction cross section on the same footing as the present model.

III. η -NUCLEUS OPTICAL POTENTIALS

As discussed in the previous section, with the sufficient reduction of the N - N^* mass gap, the level crossing between the η and N^* -hole modes takes place at a certain density in nuclear matter. As a consequence of the level crossing, the in-medium η self-energy has a strong energy dependence. In addition, this mass gap reduction as density increases gives also a strong density dependence on the η self-energy and then on the η optical potential as pointed out in Ref. [9]. The detailed discussions the η -nucleus optical potentials we used are described in Refs. [9,10,18,20].

To describe the in-medium properties of N^* , we use two kinds of the chiral models, which are based on distinct physical pictures of N^* . One is the chiral doublet model [35–37], in which N^* is regarded as the chiral partner of the nucleon. The other is the chiral unitary model, in which N^* is introduced as a dynamically generated resonance in the coupled channel meson-baryon scattering [16,17].

In the first approach, N^* is introduced as a particle with a large width and appears in an effective Lagrangian together with the nucleon field in linear realization of chiral symmetry. The η -nucleus optical potential can be obtained from the η self-energy (2):

$$\begin{aligned} V_\eta(\omega, r) &= \frac{\Pi_\eta(\omega, k=0; \rho(r))}{2\mu} \\ &= \frac{g_\eta^2}{2\mu} \frac{\rho(r)}{\omega + m_N^*(\rho(r)) - m_{N^*}^*(\rho(r)) + i\Gamma_{N^*}(\omega, \rho(r))/2} \\ &\quad + (\text{crossed term}). \end{aligned} \quad (5)$$

Here we use the local density approximation and the heavy baryon limit [14], and the density-dependent mass difference $m_N^* - m_{N^*}^*$ are given in Eq. (4). We can ignore the momentum k of the η meson because we consider almost recoilless production of the η meson in the following sections. We use an empirical density distribution of nucleons in Woods-Saxon form:

$$\rho(r) = \frac{\rho_0}{1 + \exp\left(\frac{r-R}{a}\right)}, \quad (6)$$

with $R = 1.18A^{1/3} - 0.48$ fm and $a = 0.5$ fm with the nuclear mass number A .

The optical potential (5) is sensitive to the mass difference of N and N^* in nuclei. Especially, the sign of the real part of the η optical potential changes when the mass gap of N^* and N becomes smaller than the η energy ω [9,10,18]. This means that the attractive η -nucleus interaction at low densities can turn to be repulsive depending on the values of the mass gap

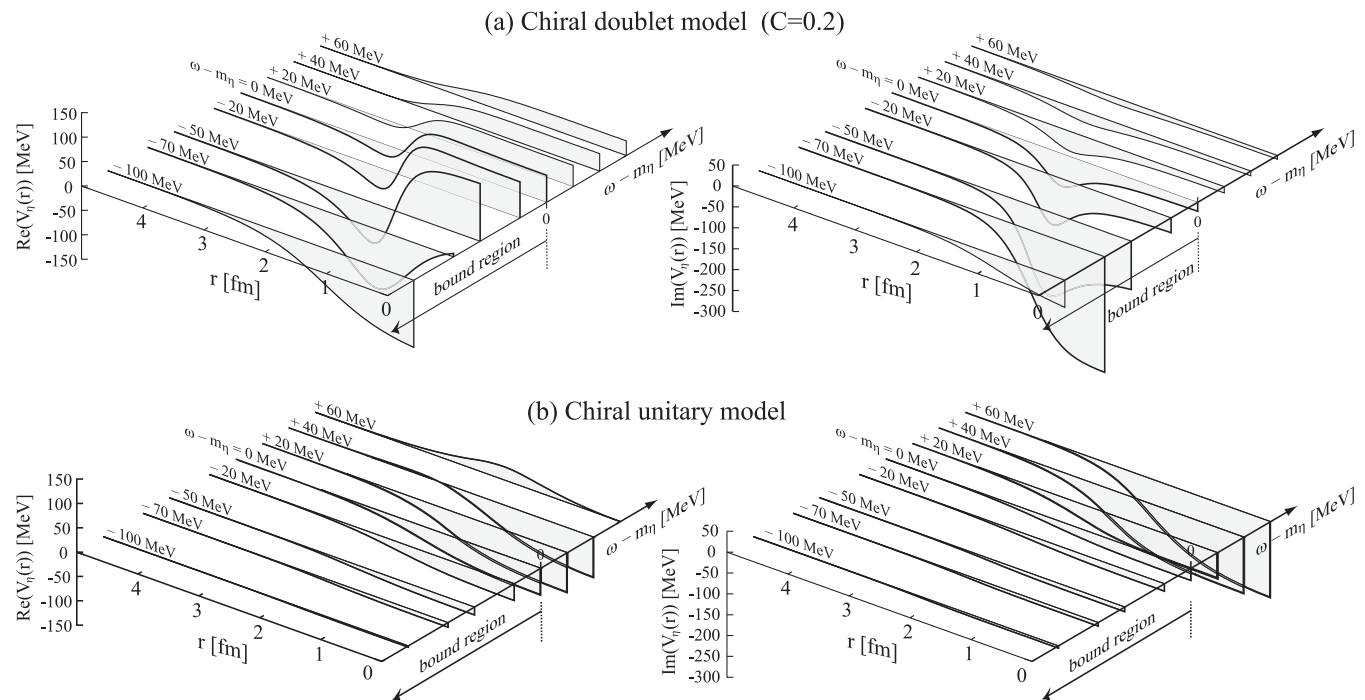


FIG. 3. The η -nucleus optical potentials with (a) the chiral doublet model ($C = 0.2$) and (b) the chiral unitary model as functions of the radial coordinate r for η energies $\omega - m_\eta = -100, -70, -50, -20, 0, +20, +40, +60$ MeV. Left and right figures show the real and imaginary parts of the optical potentials V_η , respectively.

and the η energy. This feature can be seen in Fig. 3(a), where we plot the η -nucleus optical potentials as functions of radial coordinate r at η energies. For instance, at the η threshold $\omega - m_\eta = 0$, the optical potential has a repulsive core inside the nucleus and an attractive pocket on the surface. Furthermore, this mass reduction yields also the strong energy dependence of the η -nucleus optical potential as shown in Fig. 3(a). At $\omega - m_\eta \simeq -100$ MeV, the real part of the optical potential is about 140 MeV attractive while that of the η threshold $\omega - m_\eta = 0$ is 55 MeV repulsive at $r = 0$.

To discuss the experimental feasibilities of the mesic-nuclei formation, it is very important to estimate the imaginary parts of the optical potentials. As for the N^* width in the medium that is the source of the imaginary potentials in the present model, we consider the two dominant decay channels of N^* as $N^* \rightarrow N\pi$ and $NN^* \rightarrow NN\pi$ [9,10,14] in the optical potential with the chiral doublet model. There are other possible decay modes; for instance, $N^* \rightarrow N\eta$, $N^* \rightarrow N\pi\pi$, and $N^*N \rightarrow NN$. The last two processes are strongly suppressed in nuclear matter as discussed in Refs. [9,14]. The $N^* \rightarrow N\eta$ decay is forbidden by the Pauli principle below the η threshold and the decay width at higher energy region has turned out to be negligibly small as discussed in Ref. [20]. The detailed evaluation of the N^* width in the chiral doublet model is given in Ref. [20].

In the chiral doublet model, there are two possible models concerning the assignment of the axial charge: the naive and mirror assignments [36,37]. These two models have the same density dependence of the mass gap $m_N^*(\rho) - m_{N^*}^*(\rho)$, while they show different density dependence of the in-medium

πNN^* coupling [48]. Although the in-medium N^* widths are different in these models, we have found no significant difference between the formation spectra obtained in these models [10,18], because the essential feature of the formation spectra are determined by the density dependence of the mass gap. In this article, we show only the results with the naive assignment of the chiral doublet model, which gives a larger N^* decay width in the nuclear medium than that obtained by the mirror model.

In the second approach to describe the $N^*(1535)$ resonance, which is the chiral unitary model, the optical potential has quite different features from the previous case. In this model, it was found that N^* has a dominant component of the $K\Sigma$ channel [49–51]. Because the Σ hyperon is free from the Pauli blocking in the nuclear medium, only a tiny change of the mass gap is expected in the nuclear medium [15,16]. Therefore, the η optical potential is attractive in the bound energy region, $\omega \leq m_\eta$, as shown in Fig. 3(b), and has weaker energy dependence compared with that of the chiral doublet model with $C = 0.2$. As for the imaginary part of the optical potential of the chiral unitary model, more N^* decay channels are considered in the coupled-channels approach than the chiral doublet model, such as $NN^* \rightarrow NN$. As shown later, the effect coming from this difference input of the N^* decay channels turns out to be small in the formation spectra of the η -mesic nuclei. We evaluate the η optical potential in the chiral unitary model using the η self-energy obtained in Ref. [16]. In Ref. [10], we have found that the energy dependence of the optical potential in the chiral unitary approach resembles that of the chiral doublet model with $C = 0.0$. Although we have

seen different strengths of the optical potentials in magnitude, this difference have been found not to affect the formation spectra. The binding energies and widths of the η bound states obtained with the chiral unitary model are reported in Ref. [17].

In recent works [52], it was pointed out that the $N^*(1535)$ obtained in the chiral unitary model could have some components other than the state generated dynamically by meson-baryon scattering, such as genuine quark states, and that these components could be sources of the chiral partner of the $N^*(1535)$. The would-be quark components are implemented in the subtraction constants, which are model parameters in the chiral unitary approach. In the present model for $N^*(1535)$ in the nuclear medium, the subtraction constants were assumed to be fixed. This means that the genuine quark components are independent on medium modifications in this model. This could be the origin of the different predictions on the in-medium $N^*(1535)$ mass.

IV. (π, N) REACTION FOR THE FORMATION OF THE η -NUCLEUS SYSTEM

In this section, we discuss the formation spectra of the η -mesic nuclei by the (π, N) reactions and show our main numerical results.

A. Formulation

In the beginning of this section, we give the formulation to calculate the formation spectra of the η -mesic nuclei by the (π^+, p) reaction. We use the same formulation as used in Ref. [18], in which the (γ, p) reaction was discussed for the η -mesic nuclei.

To evaluate the formation cross section, we use the Green's function method [53]. In this method, the reaction cross section is assumed to be separated into the nuclear response function $R(E)$ and the elementary cross section of the $\pi^+ n \rightarrow p \eta$ process with the impulse approximation:

$$\left(\frac{d^2\sigma}{d\Omega dE} \right)_{A(\pi^+, p)(A-1)\otimes\eta} = \left(\frac{d\sigma}{d\Omega} \right)_{n(\pi^+, p)\eta}^{\text{lab}} \times R(E), \quad (7)$$

where the nuclear response function $R(E)$ is given in terms of the in-medium Green's function $G(E)$ as

$$R(E) = -\frac{1}{\pi} \text{Im} \sum_f \int d\mathbf{r} d\mathbf{r}' \mathcal{T}_f^\dagger(\mathbf{r}) G(E; \mathbf{r}, \mathbf{r}') \mathcal{T}_f(\mathbf{r}'). \quad (8)$$

Here, the summation is inclusively taken over all possible final states. The amplitude \mathcal{T}_f describes the transition of the incident π to a neutron hole and the outgoing proton:

$$\mathcal{T}_f(\mathbf{r}) = \chi_p^*(\mathbf{r}) \xi_{1/2, m_s}^* [Y_{l_\eta}^*(\hat{r}) \otimes \psi_{j_n}(\mathbf{r})]_{JM} \chi_\pi(\mathbf{r}) \quad (9)$$

with the neutron hole wave function ψ_{j_n} , the distorted waves of π and the ejected proton χ_π and χ_p , the η angular wave function $Y_{l_\eta}(\hat{r})$, and the spin wave function $\xi_{1/2, m_s}$ of the ejected proton. For the neutron hole, we use the harmonic oscillator wave function. The Green's function $G(E)$ contains the η -

nucleus optical potential in the Hamiltonian as

$$G(E; \mathbf{r}, \mathbf{r}') = \langle n^{-1} | \phi_\eta(\mathbf{r}) \frac{1}{E - H_\eta + i\epsilon} \phi_\eta^\dagger(\mathbf{r}') | n^{-1} \rangle, \quad (10)$$

where ϕ_η^\dagger is the η creation operator and $|n^{-1}\rangle$ is the neutron hole state. The Green's function $G(E, \mathbf{r}, \mathbf{r}')$ can be obtained by solving the Klein-Gordon equation with the appropriate boundary condition. Thus, the Green's function represents both the η -meson-scattering states and bound states together with the decay modes that are expressed in the imaginary part of the potential. The imaginary part of the Green's function, or the spectral function, represents the coupling strength of the η meson to each intermediate state as a function of the energy of the η meson. If there are a quasibound state of the η meson, the spectral function has a peak structure at the corresponding energy. This can be seen in the formation spectra as a signal of the bound state.

We estimate the flux loss of the injected pion and the ejected proton due to the elastic and quasielastic scattering and/or absorption processes by the target and daughter nuclei. To estimate the attenuation probabilities, we approximate the distorted waves of the incoming pion χ_π and the outgoing proton χ_p as

$$\chi_p^*(\mathbf{r}) \chi_\pi(\mathbf{r}) = \exp[i\mathbf{q} \cdot \mathbf{r}] F(\mathbf{r}), \quad (11)$$

with the momentum transfer between pion and proton $\mathbf{q} = \mathbf{p}_\pi - \mathbf{p}_p$ and the distortion factor $F(\mathbf{r})$ evaluated by

$$F(\mathbf{r}) = \exp \left[-\frac{1}{2} \sigma_{\pi N} \int_{-\infty}^z dz' \rho_A(z', b) - \frac{1}{2} \sigma_{pN} \int_z^\infty dz' \rho_{A-1}(z', b) \right]. \quad (12)$$

Here $\sigma_{\pi N}$ and σ_{pN} are the pion-nucleon and proton-nucleon total cross sections, respectively, which contain both the elastic and inelastic processes. The values of the total cross sections are taken from Ref. [46]. For the cross section $\sigma_{\pi n}$, we use isospin symmetry. $\rho_A(z, b)$ is the density distribution function for the nucleus with the mass number A in cylindrical coordinates. In the estimation of the distortion factor, we do not take into account many-body absorptions of the initial pion, because these effects are expected to give monoenergetic minor contributions.

The calculation of the formation spectra is done separately for each subcomponent of the η -mesic nuclei labeled by $(n\ell_j)_n^{-1} \otimes \ell_\eta$, which means a configuration of a neutron-hole in the ℓ orbit with the total spin j and the principal quantum number n in the daughter nucleus and an η meson in the ℓ_η orbit. The total formation spectra are obtained by summing up these subcomponents taking into account the difference of the separation energies for the different neutron-hole states.

B. Incident pion energy and elementary cross section

We choose the incident pion energies so as to satisfy the recoil-free kinematics for the η -meson production, in which the η meson is created almost at rest in the nucleus. The good advantage of the recoil-free kinematics is that

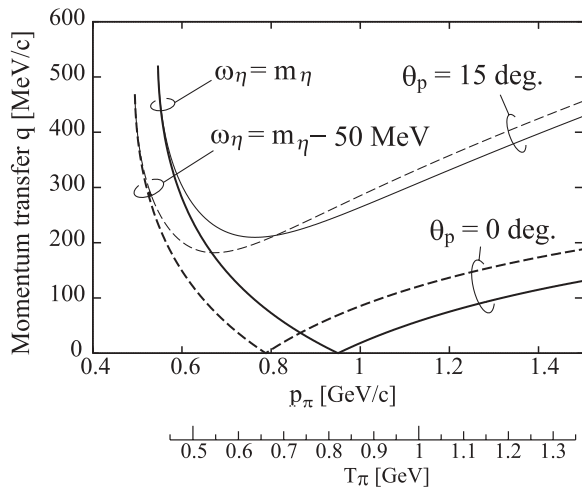


FIG. 4. Momentum transfers at the η meson energies $\omega_\eta = m_\eta$ and $m_\eta - 50$ MeV as functions of the incident pion momentum p_π . θ_p denotes the emitted proton angle in the laboratory frame. The corresponding scale of the pion kinetic energy T_π is also shown.

the formation spectra have less subcomponents due to the angular-momentum selection rule for the η and neutron hole states [6,9,10,18,20], which makes the physical interpretation of the observed spectra much easier.

In Fig. 4, we plot the momentum transfer of the $A(\pi^+, p)(A-1)_\eta$ reaction for the η energies $\omega = m_\eta, m_\eta - 50$ MeV with the proton angle being 0° and 15° as functions of the incident pion momentum and pion kinetic energy. We take the heavy mass limit for the initial and final nuclei. As Fig. 4 shows, we find that this reaction with $\theta_p = 0^\circ$ has the magic momentum where the recoilless condition is satisfied. In this article, we set the incident pion kinetic energy to be $T_\pi = 820$ MeV and $T_\pi = 650$ MeV to satisfy the recoilless condition at the η threshold and $\omega_\eta = m_\eta - 50$ MeV, respectively. These energies of the pion beam will be available at the J-PARC facility [32].

We estimate the elementary cross section $(\frac{d\sigma}{d\Omega})_{n(\pi^+, p)\eta}^{\text{lab}}$ by using the experimental data of the $\pi^- p \rightarrow n\eta$ reaction measured by the Crystal Ball Collaboration [54]. We make use of isospin symmetry to obtain the cross section of $\pi^+ n \rightarrow p\eta$ from that of the Crystal Ball data. We use the following values of the elementary cross section of $\pi^+ n \rightarrow p\eta$: $(\frac{d\sigma}{d\Omega})_{n(\pi^+, p)\eta}^{\text{lab}} = 2.4$ mb/sr for $T_\pi = 650$ MeV and $(\frac{d\sigma}{d\Omega})_{n(\pi^+, p)\eta}^{\text{lab}} = 0.64$ mb/sr for $T_\pi = 820$ MeV. The former value is read from the existing experimental data, whereas the latter is taken from the partial-wave analysis (PAW) labeled by I375 [54], which is almost equivalent to the PAW FA02 [55].

C. Numerical results of the inclusive (π, N) spectra

In Fig. 5(1), we show the calculated $^{12}\text{C}(\pi^+, p)^{11}\text{C} \otimes \eta$ cross sections for the formation of the η - ^{11}C system with the chiral doublet model potential for $C = 0.2$ [upper panel in Fig. 5(1)] and that of the chiral unitary model [lower panel in Fig. 5(1)]. The incident pion kinetic energy T_π is 820 MeV, corresponding to the recoilless condition at the η threshold. The horizontal axis indicates the excitation energy E_{ex} defined

as,

$$E_{\text{ex}} = m_\eta - B_\eta + [S_n(j_n) - S_n(\text{ground})] \quad (13)$$

where B_η is the η binding energy and $S_n(j_n)$ the neutron separation energy from the neutron single-particle level j_n . $S_n(\text{ground})$ indicates the separation energy from the neutron level corresponding to the ground state of the daughter nucleus and $E_0 = m_\eta$. Hence $E_{\text{ex}} - E_0 = 0$ corresponds to the η production threshold with the ground-state daughter nucleus. In the figure, we show the total spectra by the solid line and the contributions from dominant subcomponents by the dashed lines, separately. We take into account the difference of the separation energy $S_n(j_n) - S_n(\text{ground}) = 18$ MeV for a subcomponent accompanied by a $(0s_{1/2})_n^{-1}$ hole-state. In such a case, the η -meson production threshold appears at $E_{\text{ex}} - E_0 = 18$ MeV as indicated in Fig. 5 by the vertical dotted line. The Fig. 5(1) shows that the spectra are dominated by two contributions, $(0s_{1/2})_n^{-1} \otimes s_\eta$ and $(0p_{3/2})_n^{-1} \otimes p_\eta$, because the final states with the total spin $J \sim 0$ are largely enhanced under the recoil-free kinematics.

Let us see the spectra around the threshold; $-50 \text{ MeV} \lesssim E_{\text{ex}} - E_0 \lesssim 50 \text{ MeV}$. The spectra in this energy region were already shown in the case of the $(d, ^3\text{He})$ and (γ, p) reactions in Refs. [9,10,18]. The present work confirms that the spectral shape is very similar with the previous calculations showing that the structure of the formation spectra is not sensitive to the reaction mechanism. As already discussed in detail in Refs. [9,10,18], the spectra with the (π^+, p) reaction around the η production threshold show that the repulsive nature of the optical potential in the chiral doublet model shifts the spectra into the higher-energy region, whereas the spectra obtained in the chiral unitary model is shifted into the lower-energy region as a result of its attractive potential.

We conclude that the difference between the expected spectra with two chiral models seems to be visible in the (π^+, p) reaction as well as the (γ, p) reaction in spite of the distortion effect for the injected particle π .

In the case with the chiral doublet model, we can see the cusp structure in the $(0s_{1/2})_n^{-1} \otimes s_\eta$ subcomponent at $E_{\text{ex}} - E_0 = 18$ MeV corresponding to the η threshold for the $(0s_{1/2})_n^{-1}$ hole states. This is the so-called s -wave resonance that is found in the case with weak attraction. In this case with the chiral doublet model, the surface attractive pocket in the optical potential at the threshold causes the threshold cusp. In other words, we might be able to obtain an evidence of the curious shape of the optical potential in the doublet model from the spectral broadening into the higher-energy region (associated with the repulsion) together with the cusp structure at the threshold (associated with the weak attraction), if we could observe it. However, we should mention here that the s -hole state, corresponding to the excited state of the daughter nucleus, has natural width that is not taken into account in the present calculations. By considering the width of the s -hole state, the cusp structure could be smeared out from the spectrum.

Next, let us discuss the bound-state structures. As reported in Refs. [10,18], in the chiral unitary model case, we find a

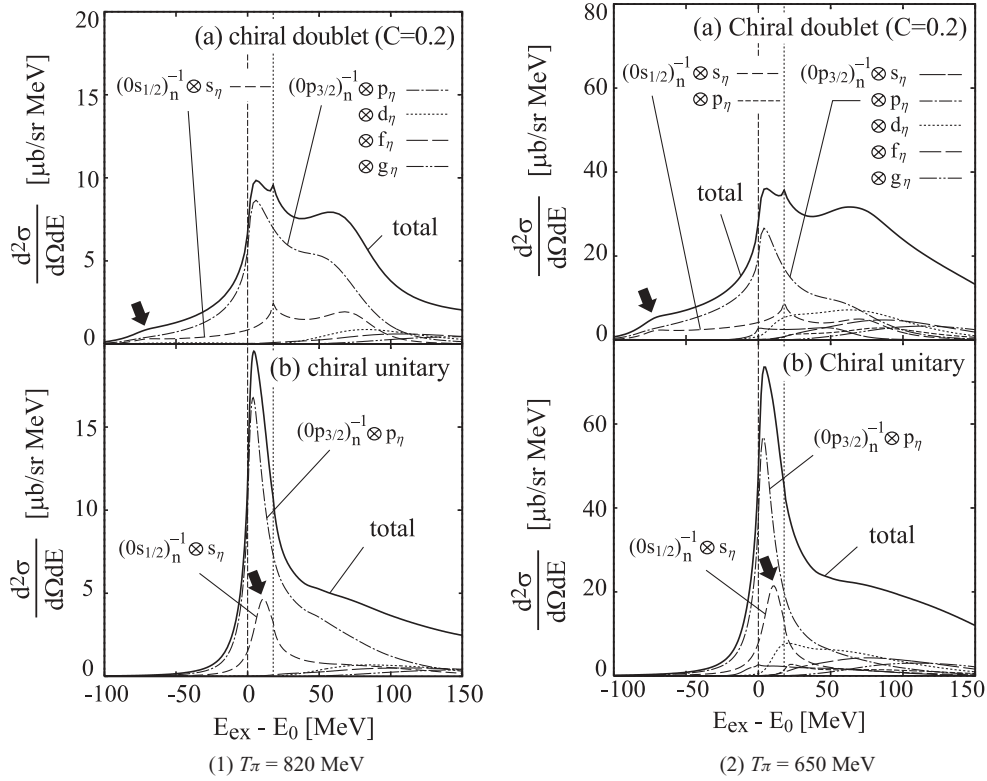


FIG. 5. Calculated spectra of the $^{12}\text{C}(\pi^+, p)^{11}\text{C} \otimes \eta$ reaction at (1) $T_\pi = 820$ MeV and (2) $T_\pi = 650$ MeV and the emitted proton angle $\theta_p = 0^\circ$ as functions of the excited energy E_{ex} . E_0 is the η production threshold. The η -nucleus interaction is calculated by using (a) the chiral doublet model with $C = 0.2$ and (b) the chiral unitary model. The thick solid lines show the total spectra and the dashed lines represent dominant subcomponents as indicated in the figures. The neutron-hole states are indicated as $(n\ell_j)_n^{-1}$ and the η states as ℓ_η . The solid arrow indicates the peak due to the bound state in each model.

bound-state peak in the subcomponent $(0s_{1/2})_n^{-1} \otimes s_\eta$ around $E_{\text{ex}} - E_0 \sim 10\text{--}15$ MeV ($\omega_\eta - m_\eta \sim -10\text{--}-5$ MeV) as indicated in Fig. 5(1)(b). The existence of the bound state in the unitary model is predicted in Ref. [17]. As seen in the figure, however, it is impossible to observe the signal of the bound state separately, because there is a larger contribution from the $(0p_{2/3})_n^{-1} \otimes p_\eta$ subcomponent in the same energy and it masks the bound state peak in the $(0s_{1/2})_n^{-1} \otimes s_\eta$ component. The peak appearing in $(0p_{2/3})_n^{-1} \otimes p_\eta$ at the η production threshold has nothing to do with the bound state of the η meson and is produced by the threshold effect. This result also means that we should keep in mind that an experimentally observed peak does not always corresponds to a bound state and it should be compared to the theoretical calculation to be identified.

In the case of the chiral doublet model case, as reported in Ref. [20], there are some bound states obtained as solutions found in the complex-energy-plane of the Klein-Gordon equation with the optical potential (5) with $C = 0.2$.² For η with $\ell_\eta = 0$, the bound states were found with the eigenenergies (B.E., Γ) = (91.3, 26.3) MeV for $0s$ and (75.1, 33.0) MeV for $1s$ [20]. In Fig. 5 we can see that the $0s$ bound state appears in the spectrum as a small bump around $E_{\text{ex}} - E_0 \sim -70\text{--}$

-80 MeV. These deep bound states correspond to the lower mode mentioned in Sec. II in the chiral doublet model ($C = 0.2$). However, the strength of the bump in the spectrum is too small to be observed in real experiments. The η bound states with $\ell_\eta = 1$ were also obtained at (79.3, 31.1) MeV for $0p$ and (72.1, 34.2) MeV for $1p$. The corresponding peak structure to the $0p$ bound state is not seen in the spectrum again due to its small strength. In the recoilless kinematics, the $1s$ and $1p$ bound states should give much less contributions in the spectrum, because there are no $1s$ - and $1p$ -hole states in the daughter nucleus for the carbon target case.

Much more prominent structure is seen in the quasifree region $E_{\text{ex}} - E_0 > 0$ in the case of the chiral doublet model. As also discussed in detail in Ref. [20], we see a considerably large bump structure around $E_{\text{ex}} - E_0 \sim 60$ MeV as shown in Fig. 5(1)(a). This peak comes from the N^* -hole mode coupled to the η meson in the medium, namely the upper mode shown in Fig. 1(b). As discussed in Sec. II, the upper mode in the chiral doublet model is enhanced as a consequence of the level crossing associated with the reduction of the N - N^* mass gap in nuclear matter stemming from the partial restoration of chiral symmetry. However, in the case of the chiral unitary approach, we see only a smooth slope in the quasifree region. Hence, the enhancement in the quasifree region could be a signal for the reduction of the N - N^* mass gap in the nuclear medium, which supports the scenario of the partial restoration of chiral symmetry in the nuclear medium. In addition, as we

²In Ref. [9], we did not search bound states with the chiral doublet potential $C = 0.2$ in energies $\omega - m_\eta \lesssim -50$ MeV, because such deep energies were out of scope of investigation in Ref. [9].

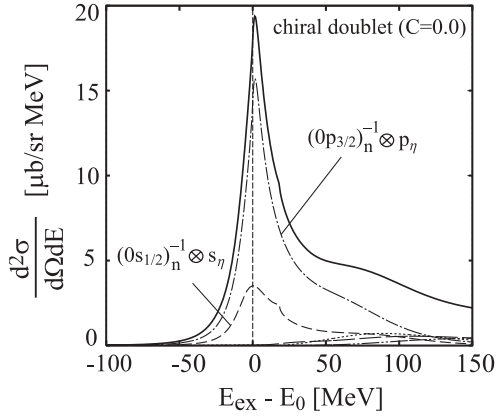


FIG. 6. Calculated spectrum of the $^{12}\text{C}(\pi^+, p)^{11}\text{C} \otimes \eta$ reaction at $T_\pi = 820$ MeV and the emitted proton angle $\theta_p = 0^\circ$ as a function of the excited energy E_{ex} . E_0 is the η production threshold. The η -nucleus interaction is calculated by using the chiral doublet model with $C = 0.0$. The thick solid line shows the total spectrum and the dashed lines represent dominant subcomponents as indicated in the figures. The neutron-hole states are indicated as $(n\ell_j)_n^{-1}$ and the η states as ℓ_η .

discussed in Sec. II, it is interesting that the peak is located at very similar energy of the N^* -hole in low densities. With this peak, the medium effect on the $N^*(1535)$ could be seen very small, as seen in η photoproduction. Nevertheless, in the present model, this spectrum shape is a consequence of the strong medium effect of the level crossing.

In Fig. 6, we show the calculated spectrum with $T_\pi = 820$ MeV in the chiral doublet model with $C = 0.0$, where the mass gap between N and N^* does not change in the nuclear medium. We find that the shape is similar to that of the chiral unitary approach shown in Fig. 5(1)(b). As mentioned in Sec. III, this means the main difference between two models shown in Fig. 5 comes from the different behaviors of the mass gap and the different input for the N^* decay width in this study does not affect the spectral shape largely.

Finally, we mention the incident pion energy dependence of the spectra. In Fig. 5(2), we show the spectra with $T_\pi = 650$ MeV corresponding to the recoilless condition at $\omega_\eta - m_\eta \sim -50$ MeV. By setting the recoilless there, we have expected some enhancement of the deep bound state in the chiral doublet model. However, although a small enhancement of the bound state can be seen, its effect is not large enough to make this bump clearly observed.

In the $T_\pi = 650$ MeV case, we find that the magnitude of the cross section is four times larger than that of $T_\pi = 820$ MeV, because of the larger elementary cross section at this energy. We also find that, due to the relatively large momentum transfer (~ 100 MeV/c) at $T_\pi = 650$ MeV, many subcomponents give finite contributions at the quasifree region, while in the $T_\pi = 820$ MeV case only two subcomponent $(0p_{3/2})_n^{-1} \otimes p_\eta$ and $(0s_{1/2})_n^{-1} \otimes s_\eta$ contribute at almost all energy region shown there.

D. Spectra for πN coincident observation

As discussed in next section in detail, the formation of the η -mesic nuclei by the (π^+, p) reaction was performed at

Brookhaven at 1988 [23]. They estimated the signal-noise ratio at that experiment to be about 1/10 and considered that the background was due to nuclear protons ejected by quasifree knockout, multiple pion and proton scattering, and pion absorption. These backgrounds would be also expected in the present setup for the (π^+, p) reaction in this article. To subtract such large backgrounds, it is useful to take some coincident measurements accompanying the η -meson production in nuclei, for example, simultaneous observation of the $N\pi$ pair coming from the N^* decay in a nucleus [28,29].

In the Green's function method [53], one can separately calculate each contribution to the spectrum coming from the different η processes. On the prescription of Ref. [53], we rewrite equivalently the imaginary part of the Green's function of η as

$$\text{Im}G = (1 + G^\dagger V_\eta^\dagger) \text{Im}G_0 (1 + V_\eta G) + G^\dagger \text{Im}V_\eta G, \quad (14)$$

where G and G_0 denote the full and free Green's functions for η and V_η is the η -nucleus optical potential. The first term of the right-hand-side of Eq. (14) represents the contribution from the escape η from the daughter nucleus and the second term describes the conversion process caused by the η absorption into the nucleus. By evaluating only the conversion part, we obtain spectra associated with decays (or absorptions) of the η mesons in the nucleus, which correspond to the coincident measurements in real experiments.

In the chiral doublet model, we take into account two decay channels of N^* in the nuclear medium as mentioned in Sec. III; $N^* \rightarrow N\pi$ and $N^*N \rightarrow NN\pi$. We can separate the conversion spectrum further into two terms by dividing the imaginary potential as

$$\text{Im}V_\eta = \text{Im}V_\eta(N^* \rightarrow N\pi) + \text{Im}V_\eta(N^*N \rightarrow NN\pi), \quad (15)$$

in Eq. (14).

As shown in Fig. 7(a), we decompose the total spectra shown in Fig. 5(1)(a) into three parts; the contribution from the η -escape process and the conversion parts of the $N^* \rightarrow N\pi$ and $N^*N \rightarrow NN\pi$ processes. The expected spectrum with the coincidence of the $N\pi$ pair from N^* is indicated by the dotted line in the figure. The thin solid line in Fig. 7(a) includes both the one-body and two-body absorption of N^* estimated in the chiral doublet model. It is found that the $N^*N \rightarrow NN\pi$ contribution is much smaller than that of $N^* \rightarrow \pi N$. We also find that, in the doublet model case, the strength of the peak structure in the quasifree region corresponding to the N^* -hole mode is reduced to about half by taking the coincidence of the $N\pi$ pair from N^* .

In Fig. 7(b), we show the decomposition of the spectrum in the chiral unitary model. We only show the total conversion part, because decomposition of the η self-energy into different absorption processes was not shown explicitly in the chiral unitary approach [16]. We expect that the difference between the two approaches with and without the N^* mass reduction is still large even if we take the coincidence of the N^* decay. In this estimation we do not take into account any final-state interaction for emitted particles from the N^* decay in the daughter nucleus. These contributions would be important for further quantitative discussions.

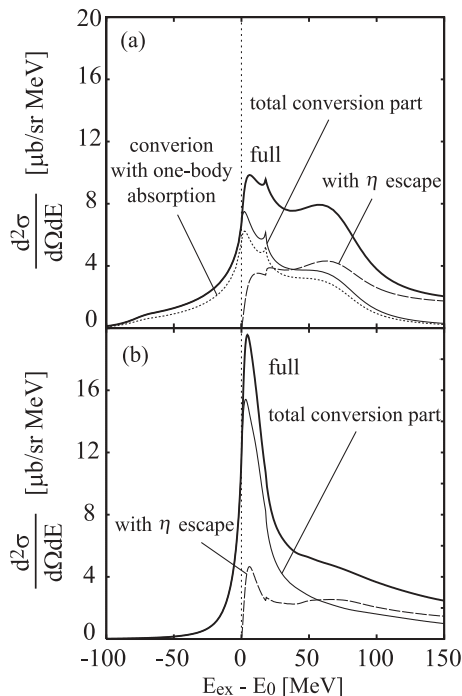


FIG. 7. Decomposition of the full spectra into the conversion parts and the escape part which are defined in the text. The reaction and energy are $^{12}\text{C}(\pi^+, p)^{11}\text{C} \otimes \eta$ and $T_\pi = 820$ MeV in (a) with the chiral doublet model and (b) the chiral unitary model. The full spectra are shown by the thick solid line and the conversion part, which includes both decay channels of $N^* \rightarrow N\pi$ and $N^*N \rightarrow NN\pi$, is shown by the thin solid line. The dashed line denotes the spectrum including only the $N^* \rightarrow N\pi$ conversion part, and the dot-dashed line denotes the escape part.

For the background estimation in experiments, it would be useful to observe the (π^-, p) process in the same setup as the (π^+, p) . In the (π^-, p) process η mesons cannot be created due to isospin symmetry, and it is expected that the formation spectra have no structure at the η -meson threshold. Such a measurement using the (π^-, p) process may be helpful for an estimation of the magnitude of the expected background and its possible structure (or shape) in the present (π^+, p) experiment.

E. Theoretical uncertainty in the present calculation

Finally, we discuss a theoretical uncertainty of the present calculation by mentioning an η -mesic nucleus formation process that we do not take into account in the present calculation. So far, we have calculated the formation spectra by considering the process in which the η meson is produced with the proton going to the forward direction in the laboratory frame. The attenuation probability of the outgoing proton has been estimated by the distortion factor given in Eq. (12), which removes all events in which the emitted proton goes to any direction after colliding with nucleons in the daughter nucleus. Suppose that the η meson is produced with a certain energy and momentum transfer and the emitted proton goes to a finite angle. The proton can come to the forward direction after collisions with nucleons in the daughter nucleus, losing its energy owing to the collisions. Such a process can be

also one of the signal processes of the η -mesic nucleus formation observed in the (π, p) reaction with the forward proton. Thus, the formation spectra of the η -mesic nucleus should be evaluated by including this rescattering process.

Let us estimate the number of such rescattering events. The number of events of the rescattering process integrated with respect to the emitted proton energy would be equivalent to that of the original forward events removed by the distortion factor, if the formation probability of the η -mesic nucleus were isotropic and the nuclear density were uniform. Based on this, we make a rough estimation of the number of events by calculating the formation cross section without the distortion factor for the outgoing proton. The calculation shows that the number of the events removed by the distortion factor is about half of the original signal events. Thus, a similar amount of events to our evaluation of the formation spectra shown in this section could come to the forward direction after the rescattering.

To see the influence of the rescattering process to our calculation of the formation spectrum, it is important to discuss the energy distribution of the rescattering process. Its energy distribution depends on the angle of the original proton before rescattering. The rescattered proton loses its energy when it changes the direction to the forward angle. The energy loss ΔE depends on the original direction and the η -meson energy. The energy loss starts from $\Delta E = 0$ MeV at an angle of zero degrees and increases monotonically as the angle increases. The maximal energy loss is around 400 MeV at 90° for the incident pion with $T_\pi = 820$ MeV. (For 15° , $\Delta E = 30$ MeV.) Therefore, the events of the rescattering process are distributed in lower proton energies, which correspond to the right side of the figures of the spectrum, than the forward proton events. For the spectrum shape of the rescattering process, we refer to Fig. 9 given in Sec. V A, which is the formation spectrum with the proton emitted to 15° angle. The spectrum shape has much less pronounced structure than with the forward proton, which satisfies the recoilless kinematics. This is because, without the recoilless condition, many combinations of the angular momenta of the η and proton-hole states contribute to the formation spectrum, and the individual spectrum structures are lost in the total spectrum. Therefore, we expect that the events of the rescattering process have rather smooth energy dependence after the integration with respect to the original proton angle. The resulting spectrum shape of the rescattering process would be smoothly distributed mainly in the quasifree region up to the proton emission threshold. If the rescattering events would make some structure in the spectrum, these events could make the bump structure appearing $E_{\text{ex}} - E_0 \sim 50$ MeV in the chiral doublet model less pronounced.

V. ADDITIONAL DISCUSSIONS ON EXPERIMENTAL FEASIBILITY

A. Comparison with the (π^+, p) reaction measured at Brookhaven

The (π^+, p) reaction experiment for the formation of the η -mesic nuclei was already performed at Brookhaven in 1988 [23]. The experiment was done at a finite proton angle

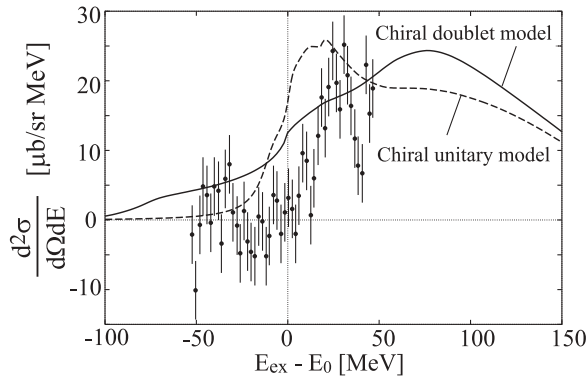


FIG. 8. Comparison of the calculated spectra and the experimental data on the carbon target case reported in Ref. [23] after the background subtraction shown in the same reference. The solid line indicates the total spectrum with the chiral doublet model ($C = 0.2$) and the dashed line is that of the chiral unitary model, calculated at the same condition with the experiment [23]. In the theoretical calculations, the angular momentum of η is taken into account up to $\ell_\eta = 6$.

$\theta_p = 15^\circ$ in the laboratory frame, based on the theoretical suggestion [11] to observe the predicted narrow bound states. The recoilless condition cannot be satisfied for finite angle proton emissions, in the case of $\theta_p = 15^\circ$, the momentum transfer is larger than $200 \text{ MeV}/c$ at any incident pion momentum as shown in Fig. 4. Therefore, the expected spectra are completely different from those of the forward angle.

We calculate the (π^+, p) spectra with the proton angle $\theta_p = 15^\circ$ and the incident pion energy $T_\pi = 673 \text{ MeV}$ ($p_\pi = 800 \text{ MeV}/c$) in the same theoretical procedure as in the previous section to compare our theoretical calculations with the experimental data obtained at Brookhaven. The comparison for the carbon target case is shown in Fig. 8. The data are taken from the second figure of Fig. 1 in Ref. [23] after the subtraction of the background estimated in the article. Because they showed an experimental error bar only for one experimental point, we assume that the single error bar is a typical error and put the same error bar to all the points. We find in Fig. 8 that both models provide the consistent results with the experimental data. This means that the experiment with the finite proton angle in Ref. [23] is not sensitive to the in-medium properties of N^* [12,13].

We show the details of the results calculated theoretically with the finite proton angle in Fig. 9. In the calculation, we take into account the η angular momenta up to $\ell_\eta = 6$. We find that, in the finite proton angle case, in contrast to the forward case, many subcomponents (especially higher-angular-momentum components $\ell_\eta \geq 1$) have substantial contributions to the total spectra. This is because the strong suppression for the configuration with the total spin $J \neq 0$, which works in the recoil-free kinematics, does not work in the finite angle case any more. This makes it difficult to interpret the spectrum structure in terms of the properties of the η and N^* in the nuclear medium.

In the spectrum calculated with the chiral unitary model, the lower panel of Fig. 9, two prominent peaks are seen around

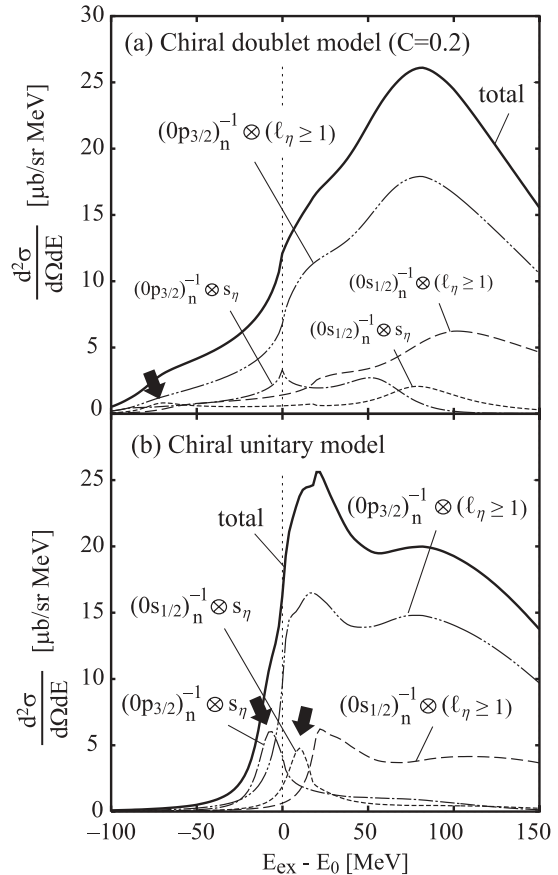


FIG. 9. Calculated spectra of the $^{12}\text{C}(\pi^+, p)^{11}\text{C} \otimes \eta$ reaction at $T_\pi = 673 \text{ MeV}$ ($p_\pi = 800 \text{ MeV}/c$) and the proton angle $\theta_p = 15^\circ$ as functions of the excited energy E_{ex} . E_0 is the η production threshold. The η -nucleus interaction is calculated by (a) the chiral doublet model with $C = 0.2$ and (b) the chiral unitary model. The thick solid lines show the total spectra and each dashed line represents the dominant subcomponent as indicated in the figures. The neutron-hole states are indicated as $(n\ell_j)_n^{-1}$ and the η states as ℓ_η . The angular momentum of η is taken into account up to $\ell_\eta = 6$. Solid arrows indicate the peaks corresponding to the bound states.

$E_{\text{ex}} - E_0 = -10 \text{ MeV}$ in the subcomponents $(0s_{1/2})_n^{-1} \otimes s_\eta$ and $(0p_{3/2})_n^{-1} \otimes s_\eta$. In particular, it is interesting that the $(0p_{3/2})_n^{-1} \otimes s_\eta$ component is enhanced now, which is strongly suppressed in the recoil-free kinematics, and the position of the bound-state peak appearing in this component is in the bound region $E_{\text{ex}} - E_0 \leq 0$ in which the contamination from the quasifree contribution is relatively small. In fact, this observation was the original idea by Haider and Liu for the advantage of the finite proton angle experiment. As seen in the figure, however, this bound-state peak is masked by the tail of the quasifree contribution of $(0p_{3/2})_n^{-1} \otimes (\ell_\eta \geq 1)$ involving the virtual η absorption by the large imaginary potential. Thus, even if the chiral unitary model prediction of the bound state is correct, the bound-state signal cannot be observed separately from the quasifree contribution in the total spectrum in this reaction. The same situation might have occurred in the Brookhaven experiment [23]. Therefore, the attempt to separate a shallow bound state from the quasifree

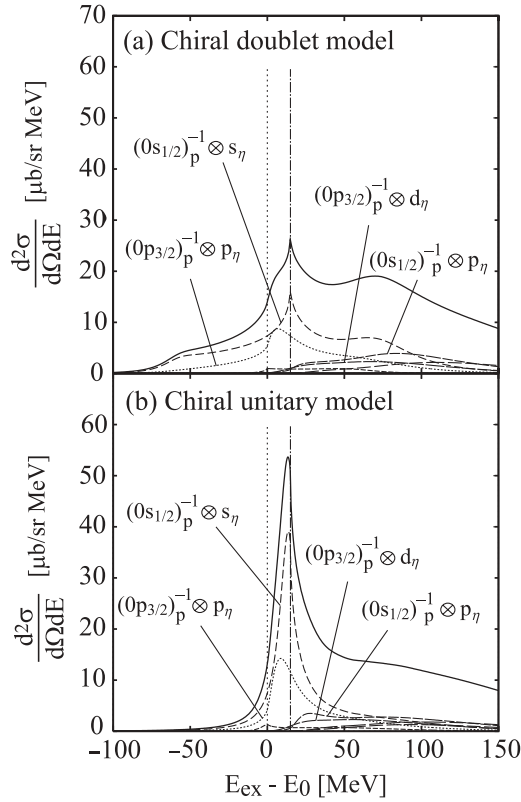


FIG. 10. Calculated spectra of the ${}^7\text{Li}(\pi^-, n){}^6\text{He} \otimes \eta$ reaction at $T_\pi = 650$ MeV and the proton angle $\theta_p = 0^\circ$ as functions of the excited energy E_{ex} . E_0 is the η production threshold. The η -nucleus interaction is calculated by (a) the chiral doublet model with $C = 0.2$ and (b) the chiral unitary model. The thick solid lines show the total spectra and each dashed line represents the dominant subcomponent as indicated in the figures. Here, the proton-hole states are indicated as $(n\ell_j)_p^{-1}$ and the η states as ℓ_η .

contribution by setting $\theta_p = 15^\circ$ seems not to work when the imaginary potential is large.

The energy range measured by the experiment [23] did not cover the energy range that we are interested in, in which the interesting features may take place, like the deep bound state and the bump structure in the quasifree region caused by the possible level crossing phenomena.

By all considerations mentioned above, we think that it is better to set the final proton angle to be zero degrees where the difference reflecting the distinct in-medium N^* properties expected to be larger and to measure a wider energy range than in the past experiment [23].

B. (π^-, n) reaction with ${}^7\text{Li}$ target

Here we show the formation spectra of the η -mesic nuclei in the (π^-, n) reaction with the ${}^7\text{Li}$ target case. As shown in Figs. 5(1) and 5(2) for the carbon target, the total spectra were dominated by the p -wave components $(0p_{2/3})_n^{-1} \otimes p_\eta$ because the target nucleus ${}^{12}\text{C}$ has four neutrons in the p state while two in the s state. Then, the s -wave components are relatively small, which contain the interesting structure such as the bound states and/or the threshold cusp.

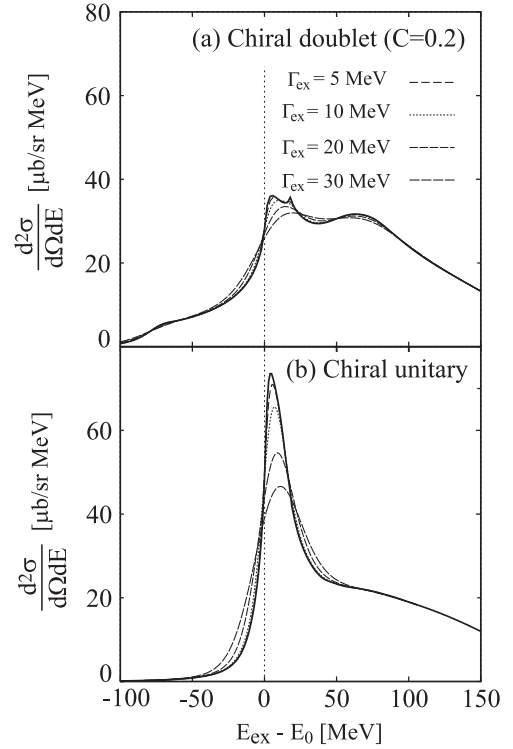


FIG. 11. Convolutions of the spectra of the ${}^{12}\text{C}(\pi^+, p){}^{11}\text{C} \otimes \eta$ reaction at $T_\pi = 650$ MeV and the proton angle $\theta_p = 0^\circ$. The thick solid lines indicate the spectra without convolution, and other lines are spectra with finite experimental resolution Γ_{ex} indicated in the figures.

In Fig. 10, we show the spectra of the ${}^7\text{Li}(\pi^-, n)$ reaction with the elementary process $\pi^- p \rightarrow n\eta$ (one proton picked-up). We see that the s -wave component now dominates the spectrum for each case (a) and (b), because ${}^7\text{Li}$ has a single proton in the p state. We can find a deep bound state peak in the s_η state around $E_{\text{ex}} - E_0 \sim -60$ MeV in the chiral doublet model also in ${}^7\text{Li}$ target case while in the chiral unitary case we can see only the threshold peak structure. We consider that the experimental data with the ${}^7\text{Li}$ target would be useful and be a good complement to that of ${}^{12}\text{C}$.

C. Consideration of finite experimental resolution

We also estimate an effect of the finite experimental energy resolution on the spectra. For this purpose, we fold the calculated spectra with $T_\pi = 650$ MeV, which is shown in Fig. 5(2), as

$$\int f(E')g(E - E')dE', \quad (16)$$

where $f(E')$ represents the calculated spectra and $g(E)$ expresses the effect of the finite energy resolution given in a Gaussian form as

$$g(E - E') = \frac{1}{a\sqrt{\pi}} \exp\left[-\left(\frac{E - E'}{a}\right)^2\right] \quad (17)$$

with $a = \Gamma_{\text{ex}}/2\sqrt{\ln 2}$. The experimental resolution (full width at half maximum) is denoted by Γ_{ex} . In Fig. 11, we show the calculated results with several energy resolutions. We can observe the difference of two approaches with $\Gamma_{\text{ex}} \sim 20$ MeV, which are expected to be reached at the J-PARC facility [32].

VI. CONCLUSION

We studied the η -mesic nuclei formation of the (π, N) reactions with nuclear targets to discuss the experimental feasibility in forthcoming experiments. Emphasizing in-medium properties of the $N^*(1535)$ baryon resonance in the context of chiral symmetry, we discussed the structure of the η -mesic nuclei formation spectra. The reduction of the N - N^* mass gap in the nuclear medium was investigated by two chiral models. In the chiral doublet model, $N^*(1535)$ is regarded as a chiral partner of the nucleon and the mass gap is expected to be reduced in association with the partial restoration of chiral symmetry in the nuclear medium [9]. In the chiral unitary approach, $N^*(1535)$ is introduced as a resonance dynamically generated and described as a quasibound state of the kaon and hyperon, and the reduction of the mass gap is expected to be small in nuclear matter [15,16].

We showed the calculated spectra of the η -mesic nuclei by the (π, N) reactions. We confirmed that the magnitude of the cross section is large enough to be observed in experiments. We found that the (π, N) reactions were also appropriate to observe the interesting behaviors like deep bound states and the bump

structure at the quasifree region that can be understood by the concept of the level crossing phenomena caused by the partial restoration of chiral symmetry [20]. We conclude that we can get new information on the in-medium N^* properties through the formation of the η -mesic nuclei by the (π, N) reactions.

We also discussed the expected background and ways to reduce it by the simultaneous observation of the $N\pi$ pair from the N^* decay in medium. We found that the difference between two treatments of in-medium N^* with and without the reduction of the N - N^* mass gap are not largely affected by the coincidence observation and there is some chance to make the observation clearer.

We believe that the present theoretical results are important to stimulate both theoretical and, especially, experimental activities to study the hadron properties in medium and to obtain new information on the partial restoration of chiral symmetry in the nuclear medium.

ACKNOWLEDGMENTS

We express our thanks to E. E. Kolomeitsev for fruitful Collaboration. We also thank K. Itahashi and H. Fujioka for useful discussions from the experimental side. H. N. acknowledges support from the Japan Society for the Promotion of Science (JSPS). This work is partially supported by the Grant for Scientific Research (Nos. 18.8661, 18042001, 20028004). A part of this work was done under the Yukawa International Project for Quark-Hadron Science (YIPQS).

-
- [1] C. J. Batty, E. Friedman, and A. Gal, Phys. Rep. **287**, 385 (1997); E. Friedman and A. Gal, *ibid.* **452**, 89 (2007).
 - [2] H. Toki, S. Hirenzaki, and T. Yamazaki, Nucl. Phys. **A530**, 679 (1991); S. Hirenzaki, H. Toki, and T. Yamazaki, Phys. Rev. C **44**, 2472 (1991).
 - [3] H. Gilg *et al.*, Phys. Rev. C **62**, 025201 (2000); K. Itahashi *et al.*, *ibid.* **62**, 025202 (2000).
 - [4] H. Geissel *et al.*, Phys. Rev. Lett. **88**, 122301 (2002).
 - [5] P. Kienle and T. Yamazaki, Phys. Lett. **B514**, 1 (2001); H. Geissel *et al.*, *ibid.* **B549**, 64 (2002); K. Suzuki *et al.*, Phys. Rev. Lett. **92**, 072302 (2004).
 - [6] R. S. Hayano, S. Hirenzaki, and A. Gillitzer, Eur. Phys. J. A **6**, 99 (1999).
 - [7] K. Tsushima, D. H. Lu, A. W. Thomas, and K. Saito, Phys. Lett. **B443**, 26 (1998); K. Saito, K. Tsushima, D. H. Lu, and A. W. Thomas, Phys. Rev. C **59**, 1203 (1999).
 - [8] S. Hirenzaki, H. Nagahiro, T. Hatsuda, and T. Kunihiro, Nucl. Phys. **A710**, 131 (2002).
 - [9] D. Jido, H. Nagahiro, and S. Hirenzaki, Phys. Rev. C **66**, 045202 (2002); Nucl. Phys. **A721**, 665c (2003).
 - [10] H. Nagahiro, D. Jido, and S. Hirenzaki, Phys. Rev. C **68**, 035205 (2003).
 - [11] Q. Haider and L. C. Liu, Phys. Lett. **B172**, 257 (1986); L. C. Liu and Q. Haider, Phys. Rev. C **34**, 1845 (1986).
 - [12] M. Kohno and H. Tanabe, Phys. Lett. **B231**, 219 (1989).
 - [13] M. Kohno and H. Tanabe, Nucl. Phys. **A519**, 755 (1990).
 - [14] H. C. Chiang, E. Oset, and L. C. Liu, Phys. Rev. C **44**, 738 (1991).
 - [15] T. Waas and W. Weise, Nucl. Phys. **A625**, 287 (1997).
 - [16] T. Inoue and E. Oset, Nucl. Phys. **A710**, 354 (2002).
 - [17] C. Garcia-Recio, J. Nieves, T. Inoue, and E. Oset, Phys. Lett. **B550**, 47 (2002).
 - [18] H. Nagahiro, D. Jido, and S. Hirenzaki, Nucl. Phys. **A761**, 92 (2005).
 - [19] N. G. Kelkar, K. P. Khemchandani, and B. K. Jain, J. Phys. G **32**, L19 (2006).
 - [20] D. Jido, E. E. Kolomeitsev, H. Nagahiro, and S. Hirenzaki, Nucl. Phys. **A811**, 158 (2008).
 - [21] C. Y. Song, X. H. Zhong, L. Li, and P. Z. Ning, Europhys. Lett. **81**, 42002 (2008).
 - [22] J. Yamagata, H. Nagahiro, and S. Hirenzaki, Phys. Rev. C **74**, 014604 (2006).
 - [23] R. E. Chrien *et al.*, Phys. Rev. Lett. **60**, 2595 (1988).
 - [24] J. Berger *et al.*, Phys. Rev. Lett. **61**, 919 (1988).
 - [25] J. D. Johnson *et al.*, Phys. Rev. C **47**, 2571 (1993).
 - [26] M. Pfeiffer *et al.*, Phys. Rev. Lett. **92**, 252001 (2004).
 - [27] C. Hanhart, Phys. Rev. Lett. **94**, 049101 (2005).
 - [28] G. A. Sokol and V. A. Tryaschev, Bull. Lebedev Phys. Inst. **1991N4**, 21 (1991) [Kratk. Soobshch. Fiz. **4**, 23 (1991)\SPLRD, 4, 21–24. 1991]; G. A. Sokol, T. A. Aibergenov, A. V. Kravtsov, A. I. L'vov, and L. N. Pavlyuchenko, Fizika B **8**, 85 (1999).
 - [29] A. Budzanowski *et al.* (COSY-GEM Collaboration), Phys. Rev. C **79**, 012201(R) (2009); V. Jha *et al.* (GEM Collaboration), Int. J. Mod. Phys. A **22**, 596 (2007).
 - [30] V. A. Baskov *et al.*, arXiv:nucl-ex/0306011.

- [31] M. K. Anikina *et al.*, arXiv:nucl-ex/0412036.
- [32] K. Itahashi and H. Fujioka (private communication); K. Itahashi, H. Fujioka, S. Hirenzaki, D. Jido, and H. Nagahiro, letter of intent for J-PARC, "Spectroscopy of η mesic nuclei via ${}^7\text{Li}(\pi, n)$ reaction at recoilless kinematics" (2007).
- [33] T. Hatsuda and T. Kunihiro, Phys. Rep. **247**, 221 (1994); G. E. Brown and M. Rho, *ibid.* **269**, 333 (1996).
- [34] D. Jido, T. Hatsuda, and T. Kunihiro, Phys. Lett. **B670**, 109 (2008).
- [35] C. DeTar and T. Kunihiro, Phys. Rev. D **39**, 2805 (1989).
- [36] D. Jido, Y. Nemoto, M. Oka, and A. Hosaka, Nucl. Phys. **A671**, 471 (2000); Y. Nemoto, D. Jido, M. Oka, and A. Hosaka, Phys. Rev. D **57**, 4124 (1998).
- [37] D. Jido, M. Oka, and A. Hosaka, Prog. Theor. Phys. **106**, 873 (2001).
- [38] M. Rößig-Landau *et al.*, Phys. Lett. **B373**, 45 (1996).
- [39] T. Yorita *et al.*, Phys. Lett. **B476**, 226 (2000).
- [40] T. Kinoshita *et al.*, Phys. Lett. **B639**, 429 (2006).
- [41] T. Maruyama and S. Chiba, Prog. Theor. Phys. **111**, 229 (2004).
- [42] J. Lehr, M. Post, and U. Mosel, Phys. Rev. C **68**, 044601 (2003).
- [43] B. Krusche, I. Jaegle, and T. Mertens, Eur. Phys. J. A **31**, 485 (2007).
- [44] T. Mertens *et al.* (The CBELSA/TAPS Collaboration), Eur. Phys. J. A **38**, 195 (2008).
- [45] B. Krusche, J. Lehr, F. Bloch, M. Kotulla, V. Metag, U. Mosel, and S. Schadmand, Eur. Phys. J. A **22**, 347 (2004).
- [46] C. Amsler *et al.* (Particle Data Group), Phys. Lett. **B667**, 1 (2008).
- [47] T. Hatsuda, T. Kunihiro, and H. Shimizu, Phys. Rev. Lett. **82**, 2840 (1999).
- [48] H. c. Kim, D. Jido, and M. Oka, Nucl. Phys. **A640**, 77 (1998).
- [49] N. Kaiser, P. B. Siegel, and W. Weise, Phys. Lett. **B362**, 23 (1995).
- [50] T. Inoue, E. Oset, and M. J. Vicente Vacas, Phys. Rev. C **65**, 035204 (2002).
- [51] E. E. Kolomeitsev and M. F. M. Lutz, Phys. Lett. **B585**, 243 (2004).
- [52] T. Hyodo, D. Jido, and A. Hosaka, Phys. Rev. C **78**, 025203 (2008); D. Jido, T. Hyodo, and A. Hosaka, Mod. Phys. Lett. A **23**, 2389 (2008).
- [53] O. Morimatsu and K. Yazaki, Nucl. Phys. **A435**, 727 (1985); **A483**, 493 (1988).
- [54] S. Prakhov *et al.*, Phys. Rev. C **72**, 015203 (2005).
- [55] R. A. Arndt, W. J. Briscoe, I. I. Strakovsky, R. L. Workman, and M. M. Pavan, Phys. Rev. C **69**, 035213 (2004).